

FGFRFT: Fast Graph Fractional Fourier Transform via Fourier Series Approximation

Ziqi Yan, Sen Shi, Feiyue Zhao, Manjun Cui, Yangfan He, and Zhichao Zhang, *Member, IEEE*

Abstract—The graph fractional Fourier transform (GFRFT) generalizes the graph Fourier transform (GFT) but suffers from a significant computational bottleneck: determining the optimal transform order requires expensive eigendecomposition and matrix multiplication, leading to $O(N^3)$ complexity. To address this issue, we propose a fast GFRFT (FGFRFT) algorithm for unitary GFT matrices based on Fourier series approximation and an efficient caching strategy. FGFRFT reduces the complexity of generating transform matrices to $O(2LN^2)$ while preserving differentiability, thereby enabling adaptive order learning. We validate the algorithm through theoretical analysis, approximation accuracy tests, and order learning experiments. Furthermore, we demonstrate its practical efficacy for image and point cloud denoising and present the fractional specformer, which integrates the FGFRFT into the specformer architecture. This integration enables the model to overcome the limitations of a fixed GFT basis and learn optimal fractional orders for complex data. Experimental results confirm that the proposed algorithm significantly accelerates computation and achieves superior performance compared with the GFRFT.

Index Terms—Graph signal processing, GFRFT, Fourier series approximation, FGFRFT.

I. INTRODUCTION

IN recent years, graph signal processing (GSP) has emerged as a powerful theoretical framework for analyzing high-dimensional data in irregular domains, such as social networks, biological systems, and sensor data [1]–[4]. It has been widely applied to tasks such as filtering, sampling, and reconstruction [5]–[11]. As the cornerstone of GSP, the graph Fourier transform (GFT) is the fundamental tool for transforming graph signals from the vertex domain to the spectral domain. Building on this foundation, researchers have generalized the GFT to the graph fractional Fourier transform (GFRFT) by introducing the concept of transform order. The GFRFT can transform graph signals

This work was supported in part by the Open Foundation of Hubei Key Laboratory of Applied Mathematics (Hubei University) under Grant HBAM202404; in part by the Foundation of Key Laboratory of System Control and Information Processing, Ministry of Education under Grant Scip20240121; and in part by the Startup Foundation for Introducing Talent of Nanjing Institute of Technology under Grant YKJ202214. (*Corresponding author: Zhichao Zhang.*)

Ziqi Yan, Sen Shi, Feiyue Zhao, and Manjun Cui are with the School of Mathematics and Statistics, Nanjing University of Information Science and Technology, Nanjing 210044, China (e-mail: yanziqi54@gmail.com; 202312380032@nuist.edu.cn; 202511150010@nuist.edu.cn; cmj1109@163.com).

Yangfan He is with the School of Communication and Artificial Intelligence, School of Integrated Circuits, Nanjing Institute of Technology, Nanjing 211167, China, and also with the Jiangsu Province Engineering Research Center of IntelliSense Technology and System, Nanjing 211167, China (e-mail: Yangfan.He@njit.edu.cn).

Zhichao Zhang is with the School of Mathematics and Statistics, Nanjing University of Information Science and Technology, Nanjing 210044, China, with the Hubei Key Laboratory of Applied Mathematics, Hubei University, Wuhan 430062, China, and also with the Key Laboratory of System Control and Information Processing, Ministry of Education, Shanghai Jiao Tong University, Shanghai 200240, China (e-mail: zzc910731@163.com).

from the vertex domain to an intermediate domain between the vertex and spectral domains, thereby offering a more flexible approach for the representation and processing of graph signals [12]–[18].

Wang et al. first established the mathematical framework for the GFRFT based on the eigendecomposition of the graph Laplacian matrix [19]. Building on this foundation, researchers have verified its superiority across multiple domains. In sampling and reconstruction, Wang and Li demonstrated that, under the optimal fractional order, signal recovery under the band-limited assumption achieves higher accuracy than the traditional GFT [20]. In filtering and signal detection, Ozturk et al. achieved efficient signal-to-noise separation for the GFRFT-domain Wiener filtering theory, whereas Cui et al. leveraged this transform to address the challenge of detecting graph linear frequency modulation signals [21], [22]. Furthermore, in data compression, Yan et al. demonstrated the advantages of fractional-domain representation for information compaction using multidimensional and multi-parameter GFRFT [23], [24]. Leveraging the dual security provided by the multi-parameter space, Cui et al. pioneered new avenues for graph signal encryption and decryption [24]. However, the determination of the transform order in these studies relies primarily on grid search strategies.

To overcome the limitations of traditional grid search in parameter determination, GFRFT is undergoing a profound shift toward a data-driven adaptive paradigm. Alikasifoglu et al. proposed an adaptive update strategy for the GFRFT transform order [25], laying the theoretical foundation for automated parameter optimization. On this basis, Yan et al. proposed a trainable joint time-vertex graph fractional Fourier transform, achieving end-to-end learning of optimal order pairs [26]. The angular GFRFT proposed by Zhao et al. demonstrated optimal denoising performance on complex data such as images and point clouds under non-stationary noise by integrating adaptive strategies for angle and order [27]. Subsequently, Sheng et al. advanced the integrated GFRFT with deep learning by proposing a generalized fractional-filtering embedding model that significantly improved performance on graph classification tasks [28]. In this context, Li et al. introduced the graph fractional Hilbert transform, which constructs precise graph-analytic signals via a parameter-adaptive update mechanism, thereby achieving a deep alignment between the feature space and task objectives in speech classification [29]. This adaptive learning mechanism significantly enhances system robustness, thereby establishing a solid foundation for the development of intelligent and adaptive GSP systems.

Despite the significant theoretical advantages of the GFRFT, determining the optimal transform order remains a major computational bottleneck in practical applications.

Existing methods for order selection typically rely on grid search or gradient descent-based updates. However, these approaches require computationally expensive eigendecomposition and dense matrix operations for each order selection or update, resulting in computational complexity as high as $O(N^3)$. This prohibitive computational cost not only restricts the scalability of the GFRFT on large-scale graph data but also severely impedes its integration as a learnable module within end-to-end deep learning frameworks.

To address this issue, focusing on unitary GFT matrices, this study proposes the FGFRFT, which combines a caching strategy with Fourier series approximation theory. This method avoids repeated eigendecomposition of the GFT matrix. By pre-caching the powers of the GFT matrix and approximating the GFRFT via Fourier series, it transforms the originally expensive matrix-matrix multiplications into efficient scalar-matrix linear combinations. This improvement reduces the computational complexity from $O(N^3)$ to $O(2LN^2)$. Crucially, this approximation process preserves full differentiability, so the transform order need not be determined via search; instead, it can be treated directly as a network parameter, enabling end-to-end adaptive learning and updating during training using gradient descent.

To comprehensively evaluate the effectiveness of the proposed algorithm, we conduct multi-faceted experimental validations. First, we analyze the numerical approximation accuracy of the algorithm and then conduct transform-order learning experiments that empirically validate its capability and convergence in dynamically updating the transform order via gradient descent. Subsequently, in image and point cloud denoising tasks, we compare the performance of our method against the traditional GFRFT, demonstrating its dual advantages in computational efficiency and processing effectiveness. Finally, to explore the algorithm's potential applications in deep learning, we replace the GFT module in the specformer [30] architecture with the GFRFT and FGFRFT modules, further evaluating its compatibility and performance as a learnable component within advanced neural network models.

The main contributions of this research are summarized as follows:

- We propose a fast approximation algorithm to mitigate the computational bottleneck of the GFRFT. By leveraging Fourier series approximation theory and a strategic caching mechanism, we successfully reduce the computational complexity from $O(N^3)$ to $O(2LN^2)$, making the fractional transform computationally efficient for large-scale graphs.
- We preserve the differentiability of the GFRFT with respect to the transform order, enabling the automatic update of the fractional order via gradient descent. This key property allows the FGFRFT to be embedded as a learnable, plug-and-play module within modern deep neural network architectures.
- We validate the effectiveness and generalization ability of the algorithm across multiple scenarios. Through numerical experiments, we verify the accuracy of the approximation and its order of convergence. In image and point cloud denoising tasks, we demonstrate the advantages of denoising. Furthermore, by integrating FGFRFT into the specformer architecture, we prove the algorithm's compatibility and performance improve-

ment within deep learning architectures.

The remainder of this research is organized as follows: Section II elaborates on the fundamental theories; Section III discusses the FGFRFT; Section IV analyses the approximation accuracy and efficiency of the method; Section V presents the experimental results; and Section VI draws the conclusions of this paper. The overall framework of the research is illustrated in Fig. 1.

II. PRELIMINARIES

A. GFT

We define a graph structure as $\mathcal{G} = (\mathcal{V}, \mathbf{A})$, where $\mathcal{V} = \{v_1, \dots, v_N\}$ contains N nodes. The weighted adjacency matrix $\mathbf{A} \in \mathbb{C}^{N \times N}$ describes the connectivity relationships between nodes, where its element $A_{m,n}$ is non-zero if and only if there exists an edge between node n and node m ; if $A_{m,n} = 0$, it indicates no connection. Typically, if $A_{m,n} = A_{n,m}$ is satisfied, the graph is considered an undirected graph [31].

A graph signal defined on the vertices of graph \mathcal{G} can be represented as a vector $\mathbf{x} \in \mathbb{C}^N$. This vector establishes a mapping from the vertex set \mathcal{V} to the complex domain \mathbb{C} , meaning the n -th element x_n in the vector corresponds to the signal value on vertex v_n .

The definition of the GFT relies on the spectral decomposition of the graph shift operator (GSO). Let $\mathbf{Z} \in \mathbb{C}^{N \times N}$ be a GSO of arbitrary form; common choices include the adjacency matrix \mathbf{A} , the Laplacian matrix \mathbf{L} , and their normalized forms [32]–[34]. The Jordan decomposition of \mathbf{Z} can be obtained as [19]:

$$\mathbf{Z} = \mathbf{V}_Z \mathbf{J}_Z \mathbf{V}_Z^{-1}, \quad (1)$$

where \mathbf{J}_Z is the Jordan normal form matrix, and the column vectors of $\mathbf{V}_Z = [\mathbf{v}_1, \dots, \mathbf{v}_N]$ constitute the generalized eigenvectors of \mathbf{Z} . Based on this, the GFT matrix is defined as the inverse of the eigenvector matrix, i.e., $\mathbf{F}_G = \mathbf{V}_Z^{-1}$.

For any graph signal \mathbf{x} , its spectral representation $\tilde{\mathbf{x}}$ in the GFT domain can be calculated via the following formula:

$$\tilde{\mathbf{x}} \triangleq \mathbf{F}_G \mathbf{x} = \mathbf{V}_Z^{-1} \mathbf{x}. \quad (2)$$

Correspondingly, the inverse graph Fourier transform (IGFT) is used to recover the graph signal from the spectral domain to the vertex domain:

$$\mathbf{x} = \mathbf{F}_G^{-1} \tilde{\mathbf{x}} = \mathbf{V}_Z \tilde{\mathbf{x}}. \quad (3)$$

B. GFRFT

The GFRFT is a generalization of the traditional GFT, aiming to introduce the theory of fractional Fourier transform from classical signal processing into the graph signal domain. Given an arbitrary graph \mathcal{G} and its GSO matrix \mathbf{Z} , we first consider the eigendecomposition form of the unitary GFT matrix \mathbf{F}_G :

$$\mathbf{F}_G = \mathbf{V}_Z^{-1} = \mathbf{V} \mathbf{\Sigma} \mathbf{V}^H, \quad (4)$$

where $\mathbf{\Sigma}$ is the Jordan form (diagonal eigenvalue matrix) of \mathbf{F}_G . Based on this, the GFRFT matrix with order $\alpha \in [0, 1]$ can be defined as:

$$\mathbf{F}_G^\alpha = \mathbf{V} \mathbf{\Sigma}^\alpha \mathbf{V}^H. \quad (5)$$

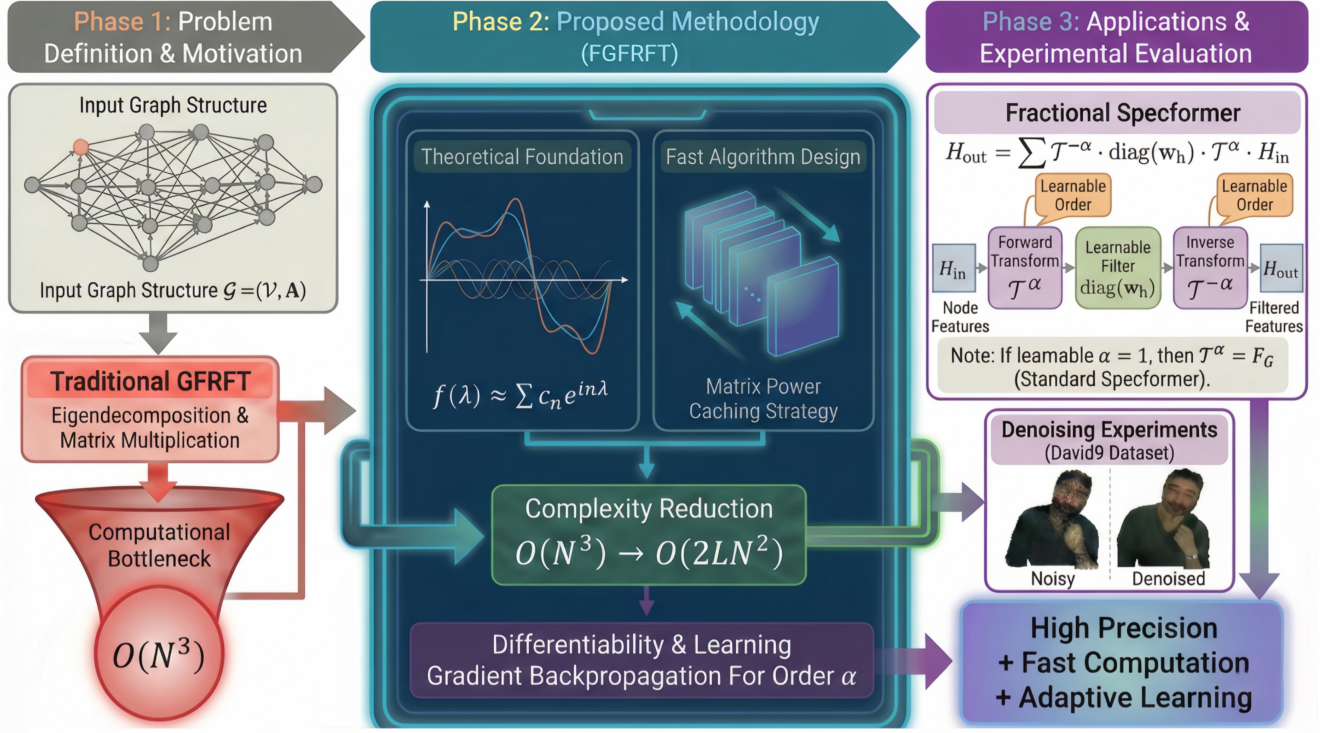


Fig. 1: Overall framework of the paper

Furthermore, to maintain consistency with the definition of classical fractional Fourier transform (FRFT) based on hyper-differential operators and to support arbitrary real-number orders $\alpha \in \mathbb{R}$, literature [25] proposes another equivalent definition:

$$\mathbf{F}_G^\alpha = \exp\left(-j\frac{\alpha\pi}{2}\left(\pi(\mathbf{D}_G^2 + \mathbf{F}_G\mathbf{D}_G^2\mathbf{F}_G^{-1}) - \frac{1}{2}\mathbf{I}_N\right)\right), \quad (6)$$

where the operator \mathbf{D}_G^2 is given by:

$$\mathbf{D}_G^2 = \frac{1}{2\pi}\left(\frac{j^2}{\pi}\log(\mathbf{F}_G) + \frac{1}{2}\mathbf{I}_N\right). \quad (7)$$

The above two definitions are essentially equivalent; both satisfy index additivity and possess desirable boundary properties: degenerating to the identity matrix \mathbf{I}_N when $\alpha = 0$, and becoming the standard GFT matrix \mathbf{F}_G when $\alpha = 1$.

C. Fourier Series Approximation Theory

The Fourier series is a core mathematical tool for analyzing periodic functions, stating that any periodic signal satisfying the Dirichlet conditions can be decomposed into a weighted sum of complex exponential functions [35]–[38].

For a square-integrable function $g(\theta)$ defined on the finite interval $[-\pi, \pi]$, we can view it as a function with a period of 2π through periodic extension. According to the Fourier series expansion, this function can be expressed as the following complex exponential series:

$$g(\theta) = \sum_{n=-\infty}^{\infty} c_n e^{jn\theta}, \quad \theta \in [-\pi, \pi], \quad (8)$$

where c_n are the Fourier coefficients, obtained via orthogonal projection:

$$c_n = \frac{1}{2\pi} \int_{-\pi}^{\pi} g(\theta) e^{-jn\theta} d\theta. \quad (9)$$

III. FGFRFT

This section focuses on the unitary property of the GFT matrix, detailing the mathematical derivation of reconstructing the GFRFT matrix using Fourier series approximation theory. We derive the corresponding fast computation formulas and analyze their computational complexity.

A. Fourier Series Expansion of GFRFT Eigenvalues

Let \mathbf{F}_G be a GFT matrix that is unitary. It can be eigendecomposed as $\mathbf{F}_G = \mathbf{V}\mathbf{\Sigma}\mathbf{V}^H$. The core operation of GFRFT involves performing fractional power operations on the diagonal matrix $\mathbf{\Sigma}$ after eigendecomposition, resulting in $\mathbf{\Sigma}^\alpha$, and then re-multiplying the matrices to obtain $\mathbf{F}_G^\alpha = \mathbf{V}\mathbf{\Sigma}^\alpha\mathbf{V}^H$.

Therefore, the GFRFT generation process requires eigendecomposition and matrix multiplication. For the eigendecomposition part, a caching strategy can be adopted, caching the required \mathbf{V} , $\mathbf{\Sigma}$, \mathbf{V}^H and only calculating $\mathbf{\Sigma}^\alpha$ to avoid repetitive decomposition of the GFT matrix. However, the complexity of the matrix multiplication stage remains high. Thus, we attempt to utilize Fourier series theory to approximate the entire calculation process.

Based on the properties of unitary matrices, their eigenvalues are distributed on the unit circle in the complex plane. Let λ_k be the k -th eigenvalue of \mathbf{F}_G , then:

$$\lambda_k = e^{j\theta_k}, \quad \theta_k \in (-\pi, \pi), \quad k = 1, \dots, N. \quad (10)$$

Accordingly, the fractional power operation on the eigenvalue matrix is equivalent to performing power operations on the eigenvalues:

$$\lambda_k^\alpha = (e^{j\theta_k})^\alpha = e^{j\alpha\theta_k}. \quad (11)$$

This indicates that the eigenvalues of GFRFT are essentially a function $g(\theta) = e^{j\alpha\theta}$ with respect to the phase angle θ .

Based on the above hypothesis, we expand $e^{j\alpha\theta}$ as a Fourier series:

$$e^{j\alpha\theta} = \sum_{n=-\infty}^{\infty} c_n(\alpha)e^{jn\theta}, \quad \theta \in (-\pi, \pi), \quad (12)$$

where the expansion coefficients $c_n(\alpha)$ are calculated as follows. Through integral operation, the analytical solution can be obtained:

$$c_n(\alpha) = \frac{1}{2\pi} \int_{-\pi}^{\pi} e^{j(\alpha-n)\theta} d\theta = \frac{\sin(\pi(\alpha-n))}{\pi(\alpha-n)}. \quad (13)$$

That is, the Fourier coefficients $c_n(\alpha)$ follow a normalized sinc function distribution.

Remark 1: It is worth noting that for non-integer orders α , the function $g(\theta) = e^{j\alpha\theta}$ exhibits discontinuity at the interval boundaries $\pm\pi$ (i.e., $e^{j\alpha\pi} \neq e^{-j\alpha\pi}$). This boundary discontinuity leads to the Gibbs phenomenon near the endpoints in the Fourier series, thereby destroying the uniform convergence of the approximation. Therefore, to ensure the accuracy and validity of the series approximation, this paper assumes that the eigenvalues of the GFT matrix do not include -1 . Under this condition, the function is a smooth continuous function within the region where all eigenvalues are distributed, satisfying the condition for uniform convergence.

B. FGFRFT Definition

Since the previous section demonstrates that the scalar function $e^{j\alpha\theta}$ can be expanded into a uniformly convergent Fourier series within the domain, we can substitute this series relation into each diagonal element of the diagonal matrix Σ^α :

$$\begin{aligned} \Sigma^\alpha &= \text{diag} \left(\sum_{n=-\infty}^{\infty} c_n(\alpha)e^{jn\theta_1}, \dots, \sum_{n=-\infty}^{\infty} c_n(\alpha)e^{jn\theta_N} \right) \\ &= \sum_{n=-\infty}^{\infty} c_n(\alpha) \cdot \text{diag}(\lambda_1^n, \dots, \lambda_N^n) \\ &= \sum_{n=-\infty}^{\infty} c_n(\alpha) \Sigma^n. \end{aligned} \quad (14)$$

Subsequently, multiplying the matrices \mathbf{V} and \mathbf{V}^H on the left and right sides of Eq. (14), respectively:

$$\begin{aligned} \mathbf{F}_G^\alpha &= \mathbf{V} \left(\sum_{n=-\infty}^{\infty} c_n(\alpha) \Sigma^n \right) \mathbf{V}^H \\ &= \sum_{n=-\infty}^{\infty} c_n(\alpha) (\mathbf{V} \Sigma^n \mathbf{V}^H) \\ &= \sum_{n=-\infty}^{\infty} c_n(\alpha) \mathbf{F}_G^n. \end{aligned} \quad (15)$$

Note that $\mathbf{V} \Sigma^n \mathbf{V}^H$ corresponds exactly to the integer power of the original GFT matrix, denoted as \mathbf{F}_G^n . Thus, we obtain the definition form of FGFRFT. This definition reveals the core computational mechanism of FGFRFT: the transformation matrix \mathbf{F}_G^α of any fractional order can be obtained by a weighted linear combination of the integer powers \mathbf{F}_G^n of the GFT matrix, where the weight coefficients $c_n(\alpha)$ are analytically determined solely by the sinc function.

Definition 1: In practical computation, we truncate the series, taking the first L terms for approximation. The matrix after truncation is defined as the order- L FGFRFT matrix:

$$\mathbf{Q}_L^\alpha = \sum_{n=-L}^L c_n(\alpha) \mathbf{F}_G^n. \quad (16)$$

Corollary 1: We utilize the property of unitary matrices $\mathbf{F}_G^{-n} = (\mathbf{F}_G^n)^{-1} = (\mathbf{F}_G^n)^H = (\mathbf{F}_G^H)^n$. By separating the positive and negative terms in the series, we derive the following efficient computation formula:

$$\mathbf{Q}_L^\alpha = c_0(\alpha) \mathbf{I}_N + \sum_{n=1}^L [c_n(\alpha) \mathbf{F}_G^n + c_{-n}(\alpha) (\mathbf{F}_G^H)^n]. \quad (17)$$

Definition 2: Given a graph signal \mathbf{x} , the action of FGFRFT on the graph signal is defined as:

$$\tilde{\mathbf{x}}_\alpha^L = \mathbf{Q}_L^\alpha \mathbf{x}. \quad (18)$$

Correspondingly, the action of IFGFRFT on the graph signal is defined as:

$$\mathbf{x} = \mathbf{Q}_L^{-\alpha} \tilde{\mathbf{x}}_\alpha^L. \quad (19)$$

Remark 2: Although the FGFRFT matrix is an approximation derived based on truncated Fourier series, when the truncation order L is selected appropriately, this matrix can maintain the properties of GFRFT, such as additivity, invertibility, and unitary property, with high precision.

Remark 3: Based on the parity properties of the sinc function, we observe that $c_n(-\alpha) = c_{-n}(\alpha)$. This mathematical property ensures it strictly satisfies conjugate symmetry, i.e., $\mathbf{Q}_L^{-\alpha} = (\mathbf{Q}_L^\alpha)^H$.

Remark 4: Regarding the differentiability of the FGFRFT matrix with respect to α , since the matrix powers \mathbf{F}_G^n are independent of α , the calculation of the gradient transforms into the derivation of the coefficients $c_n(\alpha)$:

$$\frac{\partial \mathbf{Q}_L^\alpha}{\partial \alpha} = \sum_{n=-L}^L \frac{d}{d\alpha} \left(\frac{\sin(\pi(\alpha-n))}{\pi(\alpha-n)} \right) \mathbf{F}_G^n. \quad (20)$$

Since the sinc function is smooth and differentiable everywhere in the real domain, it indicates that the gradient of the FGFRFT matrix is well-defined and has a closed form. This implies that the error gradient can be back-propagated to α_l of each layer via the chain rule, thereby realizing the adaptive update of the transform order.

C. Complexity Analysis

This section focuses on analyzing the computational complexity of the proposed algorithm versus the traditional GFRFT. For a fair comparison, we divide the computation process into two stages: offline pre-computation and online computation. Pre-computed matrices are cached, allowing direct retrieval during online computation without recalculation. Assume the number of graph nodes is N and the truncation order is L .

1) GFRFT Algorithm:

- **Offline Phase:** Requires performing eigendecomposition on the GFT matrix once to obtain the eigenvector matrix \mathbf{V} , its conjugate transpose \mathbf{V}^H , and the eigenvalue diagonal matrix Σ . The complexity of this step is $O(N^3)$, and the results are cached for subsequent use.

- **Online Phase:** When the transform order α is updated, it first requires calculating the new eigenvalue powers Σ^α with a complexity of $O(N)$. However, the primary computational bottleneck lies in reconstructing the dense matrix \mathbf{F}_G^α , i.e., executing the matrix multiplication $\mathbf{V}(\Sigma^\alpha \mathbf{V}^H)$. Even utilizing the sparsity of the diagonal matrix, the complexity of the final dense matrix multiplication remains $O(N^3)$. This implies that the traditional method is extremely inefficient in scenarios requiring frequent updates of α , such as gradient descent.

2) *FGFRFT Algorithm:*

- **Offline Phase:** The algorithm pre-constructs and caches the set of GFT matrix powers $\mathcal{C} = \{\mathbf{F}_G^n\}_{n=1}^L$. The complexity of this step is $O(LN^3)$, and the actual computational burden can be further reduced through a recursive multiplication strategy.
- **Online Phase:** When α changes, the algorithm only needs to calculate the scalar coefficients $c_n(\alpha)$, followed by executing scalar-matrix multiplication and matrix addition operations. Since the complexity of matrix addition and scalar multiplication is $O(2LN^2)$, and the truncation order L is typically much smaller than N ($L \ll N$), the total complexity of online calculation is significantly reduced to $O(N^2)$.

To clearly demonstrate this, we compare the computational complexity of the different algorithms in Table I, and provide the specific implementation pseudocode of the proposed FGFRFT in Algorithm 1, detailing the complete steps from offline caching to online linear combination. Through the caching strategy, the online computational complexity is successfully limited to $O(2LN^2)$. In large-scale graph data processing, our proposed algorithm alleviates the computational burden of traditional methods when updating the GFRFT matrix.

TABLE I: Computational Complexity Comparison

Algorithm	Pre-computation	Order Update	Dominant Operation
Traditional GFRFT	Eigen-decomposition: $O(N^3)$	$O(N^3)$	Matrix-Matrix Multiplication
Proposed FGFRFT	Matrix Powers: $O(LN^3)$	$O(2LN^2)$	Scalar-Matrix Linear Combination

IV. ANALYSIS OF APPROXIMATION ACCURACY AND COMPUTATIONAL EFFICIENCY

To validate the theoretical low complexity and numerical approximation capability of the proposed FGFRFT algorithm, we conduct benchmark tests on random unitary GFT matrices of varying scales. The standard GFRFT algorithm based on eigendecomposition served as the baseline for comparison.

A. Experimental Settings and Evaluation Metrics

1) *Software and Hardware Environment:* All experiments are conducted with a configuration of Python 3.9.21 and PyTorch 2.6.0 on a 12th Gen Intel(R) Core(TM) i5-12600KF processor (3.70 GHz). The algorithms are implemented based on Python and the PyTorch framework. To ensure the reproducibility of results, we fix the random seeds in all experiments.

Algorithm 1 FGFRFT

Require: Graph Shift Operator $\mathbf{Z} \in \mathbb{C}^{N \times N}$, Transform order $\alpha \in \mathbb{R}$, Truncation order L .

Ensure: Approximated GFRFT operator $\mathbf{Q}_L^\alpha \approx \mathbf{F}_G^\alpha$.

- 1: **Stage 1: Offline Pre-computation**
- 2: Perform eigen-decomposition: $\mathbf{Z} = \mathbf{V}\mathbf{\Lambda}\mathbf{V}^{-1}$.
- 3: Construct GFT matrix: $\mathbf{F}_G \leftarrow \mathbf{V}^{-1}$. {Assumption: \mathbf{F}_G is Unitary}
- 4: Initialize Basis Cache $\mathcal{C} \leftarrow \emptyset$.
- 5: Let $\mathbf{P}_0 = \mathbf{I}_N$.
- 6: **for** $n = 1$ to L **do**
- 7: Compute power iteratively: $\mathbf{P}_n \leftarrow \mathbf{F}_G \cdot \mathbf{P}_{n-1}$.
- 8: Store \mathbf{P}_n in \mathcal{C} .
- 9: **end for**
- 10: **Stage 2: Online Computation**
- 11: Initialize operator: $\mathbf{Q}_L^\alpha \leftarrow \text{sinc}(\alpha)\mathbf{I}_N$.
- 12: **for** $n = 1$ to L **do**
- 13: Calculate Sinc coefficients:
- 14: $c_n \leftarrow \text{sinc}(\alpha - n)$
- 15: $c_{-n} \leftarrow \text{sinc}(\alpha + n)$
- 16: Retrieve \mathbf{P}_n from Cache \mathcal{C} .
- 17: Update operator:
- 18: $\mathbf{Q}_L^\alpha \leftarrow \mathbf{Q}_L^\alpha + c_n \mathbf{P}_n + c_{-n} \mathbf{P}_n^H$.
- 19: **end for**
- 20: **return** \mathbf{Q}_L^α

2) *Evaluation Metrics:* To quantitatively evaluate the approximation performance of the proposed FGFRFT algorithm, we consider the standard GFRFT results based on eigendecomposition as the ground truth. Let N be the number of graph nodes, and the error matrix is defined as $\mathbf{D} = \mathbf{Q}_L^\alpha - \mathbf{F}_G^\alpha$. We employ the following three metrics for evaluation: Mean squared error (MSE), mean absolute error (MAE), and normalized MSE (NMSE).

$$MSE = \frac{1}{N^2} \sum_{i=1}^N \sum_{j=1}^N |D_{ij}|^2, \quad (21)$$

$$MAE = \frac{1}{N^2} \sum_{i=1}^N \sum_{j=1}^N |D_{ij}|, \quad (22)$$

$$NMSE = \frac{\|\mathbf{D}\|_F^2}{\|\mathbf{F}_G^\alpha\|_F^2}, \quad (23)$$

where $\|\cdot\|_F$ denotes the Frobenius norm of a matrix, and $|\cdot|$ denotes the modulus of a complex number.

B. Impact of Truncation Order L on Approximation Accuracy

To investigate the impact of the hyperparameter L on the algorithm's accuracy, we further analyze the error convergence under different L values ($L \in \{10, 20, 30\}$). Figs. 2, 3, and 4 illustrate the trends of MSE, MAE, and NMSE with respect to L , under combinations of different transform orders $\alpha \in \{0.15, 0.35, 0.55, 0.75, 0.95\}$ and varying node counts $N \in \{2000, 3000, 4000\}$.

It can be clearly observed from the figures that as the truncation order L increases from 10 to 100, all three error metrics exhibit a monotonic decreasing trend, validating the uniform convergence of the Fourier series approximation. When $L = 20$, the MSE error stably drops to the level

of 10^{-6} or even lower, which offers sufficient precision for the vast majority of graph signal processing tasks. Although $L = 30$ provides extremely high numerical approximation capability, considering the memory overhead of storing L power matrices, we set $L \in [10, 20]$ in practical applications to achieve the optimal trade-off between resource consumption and accuracy.

C. Comparison of Computational Efficiency on Large-Scale Graphs

We evaluate the online computational performance on graphs with node scales N increasing from 1000 to 8000. The truncation order was set to $L = 10$. For a fair comparison, the recorded time includes only the time required to construct the transformation matrix based on a given order α . The experimental results are shown in Table II.

Experimental data indicate that FGFRFT is significantly faster than the standard GFRFT across all tested scales, with the speedup ratio reaching a peak of $7.59\times$. This achievement benefits from the algorithm simplifying the complex matrix reconstruction process into an efficient cache-based linear combination. Theoretically, as N increases, the time difference between $O(N^3)$ and $O(N^2)$ should continue to widen, thereby yielding a continuously growing speedup ratio. Our experimental data validate this trend for $N \leq 7000$, where the rate rose from 1.92 to 7.59. However, at $N = 8000$, we observe a slight regression in the speedup ratio. This is attributed to the reliance on reading and summing L large cached matrices during large-scale matrix operations. When $N = 8000$, caching $L = 10$ large-scale complex matrices occupies a substantial amount of system memory, leading to memory bandwidth saturation and potential memory swapping latency. Consequently, the CPU wait time increases, causing the growth of the speedup ratio to decelerate.

TABLE II: Computation Efficiency and Approximation Accuracy Comparison between Standard GFRFT and Proposed FGFRFT ($L = 10$)

Node Size (N)	Standard GFRFT (s)	Proposed FGFRFT (s)	Speedup Ratio (\times)	MSE	MAE	NMSE
1000	0.0130	0.0068	1.92	2.05E-05	4.00E-03	2.05E-02
2000	0.0866	0.0366	2.37	1.00E-05	2.80E-03	2.01E-02
3000	0.3245	0.0845	3.84	6.58E-06	2.27E-03	1.97E-02
4000	0.7227	0.1586	4.56	4.92E-06	1.97E-03	1.97E-02
5000	1.3942	0.2484	5.61	3.98E-06	1.77E-03	1.99E-02
6000	2.3962	0.3582	6.69	3.34E-06	1.62E-03	2.00E-02
7000	3.7579	0.4952	7.59	2.83E-06	1.49E-03	1.98E-02
8000	5.5446	0.8120	6.83	2.46E-06	1.39E-03	1.57E-03

Note: The speedup ratio at $N = 8000$ reflects memory bandwidth saturation limits.

V. EXPERIMENT RESULTS

A. Transform Order Learning Experiments

This section aims to verify whether the proposed FGFRFT possesses the capability to be embedded into deep neural networks for end-to-end training. We first present the mathematical formulation of a multi-layer transform network, followed by verifying its convergence performance in gradient descent through transform order experiments.

Consider a cascaded network containing K layers of FGFRFT. Each layer functions similarly to a fully connected

layer, where the output is controlled by a single parameter. Since $\mathbf{Q}_L^{\alpha_l}$ is differentiable with respect to α_l , the backpropagation algorithm can be utilized to update the parameter α_l . Given an input graph signal \mathbf{X} , the network output $\hat{\mathbf{Y}}$ can be represented as the sequential product of each layer:

$$\hat{\mathbf{Y}} = \left(\prod_{l=1}^K \mathbf{Q}_L^{\alpha_l} \right) \mathbf{X}, \quad (24)$$

where α_l denotes the learnable transform order of the l -th layer. We define the target output signal \mathbf{Y} and the MSE loss function \mathcal{L} :

$$\mathbf{Y} = \mathbf{F}_G^{\alpha_{target}} \mathbf{X}. \quad (25)$$

$$\mathcal{L} = \frac{1}{N^2} \|\hat{\mathbf{Y}} - \mathbf{Y}\|_F^2. \quad (26)$$

The objective is to learn the optimal order for each layer such that the final MSE is minimized. We design transform order update experiments with varying numbers of layers.

The experimental setup is as follows: The network depth is set to $K \in \{1, 2, 3\}$. The initial order for each layer is initialized to $\alpha_{init} = 0.1$. The global target total order is set to $\alpha_{target} = 1.5$. \mathbf{X} is set as the identity matrix. We utilize the Adam optimizer for optimization, with a learning rate of 0.01 and 200 iterations. The experimental results are presented in Table III, showcasing the final Loss, the sum of transform orders, the error relative to the target transform order, total training time, and speedup for different layer counts. In Fig. 5, we display the Loss curve during model training and the trajectory of transform order updates. Algorithm 2 presents the pseudocode for the entire process.

TABLE III: Learning Performance Comparison with Varying Network Depths ($K \in \{1, 2, 3\}$, Target $\alpha = 1.5$)

Method	Network Depth (K)	Final Loss	Final $\sum \alpha$	Error $ \Delta\alpha $	Total Time (s)	Speedup Ratio (\times)
Proposed FGFRFT	1	5.02E-06	1.5009	0.0009	436.61	5.15
	2	7.21E-06	1.4989	0.0011	969.66	2.73
	3	1.54E-05	1.4947	0.0053	1497.06	2.78
Standard GFRFT	1	4.94E-10	1.5009	0.0009	2250.78	1.00
	2	4.81E-12	1.4999	0.0000	2650.25	1.00
	3	1.02E-11	1.5000	0.0000	4163.34	1.00

The experimental results strongly validate the differentiability and numerical stability of the proposed FGFRFT within deep network architectures. Regardless of variations in network depth, the sum of the learned transform orders $\sum \alpha$ converges rapidly and smoothly to the target ground truth, with the final parameter error stably controlled within the extremely low range of 0.0009 to 0.0053. This result not only corroborates the algorithm's approximate additivity but also reaffirms its high approximation accuracy during the dynamic optimization process. Although the convergence loss floor of FGFRFT is approximately 10^{-5} due to the inherent characteristics of series truncation, slightly higher than standard methods based on exact eigendecomposition, it trades this for a significant training speedup of $2.78 \sim 5.15\times$. This efficiency improvement, achieved with minimal precision sacrifice, demonstrates the efficiency and feasibility of embedding this algorithm as a learnable module into deep graph neural networks.

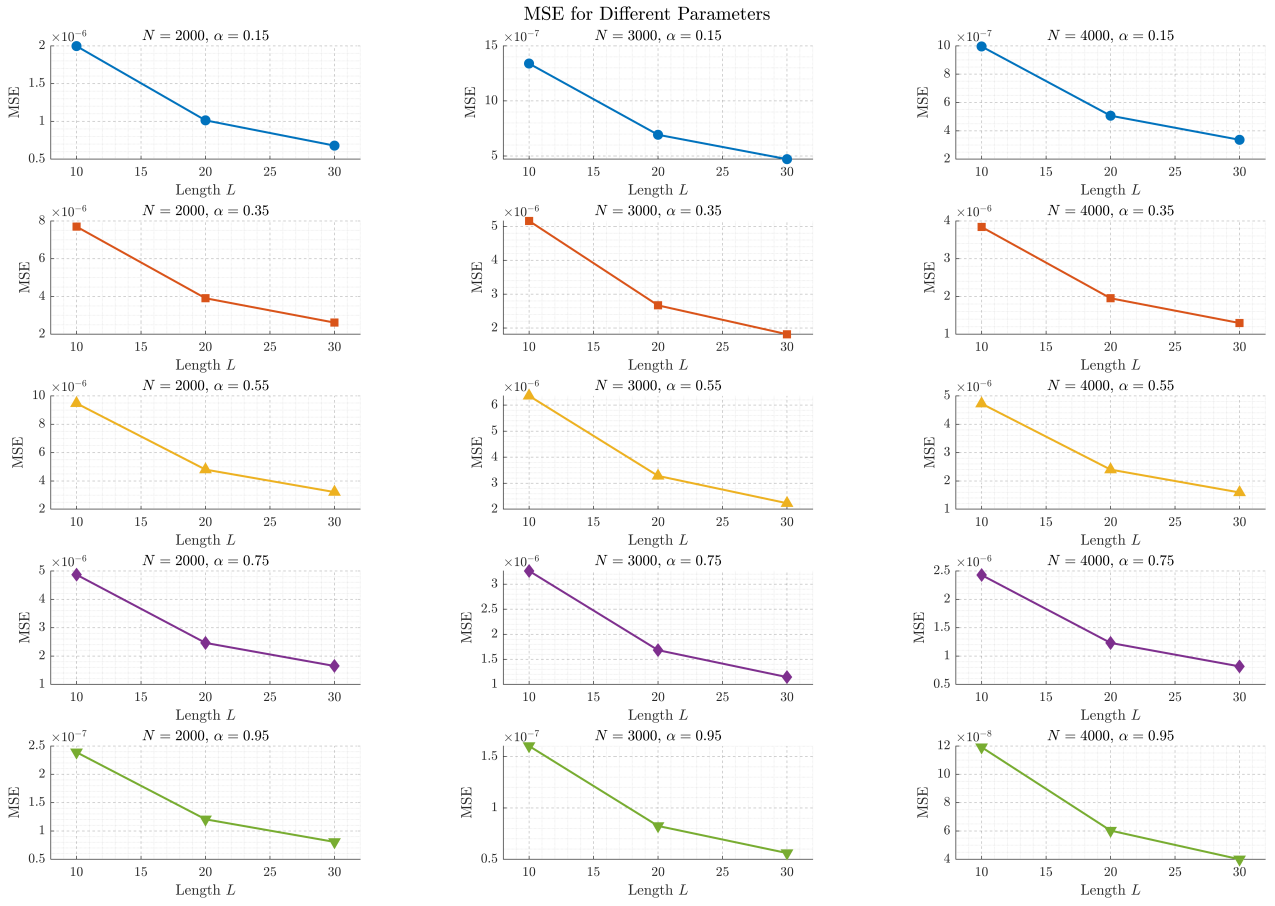


Fig. 2: The trend of MSE with respect to truncation order L .

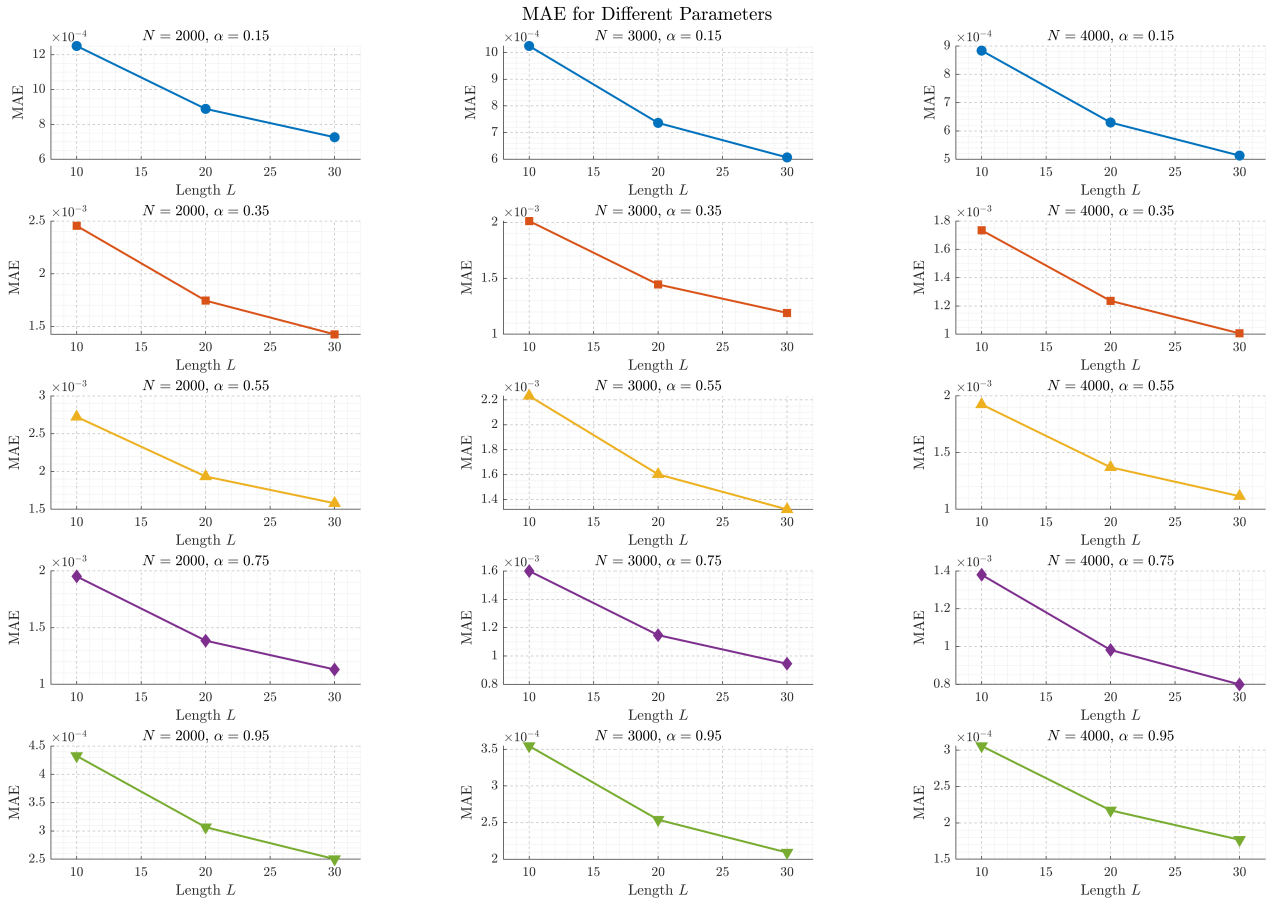


Fig. 3: The trend of MAE with respect to truncation order L .

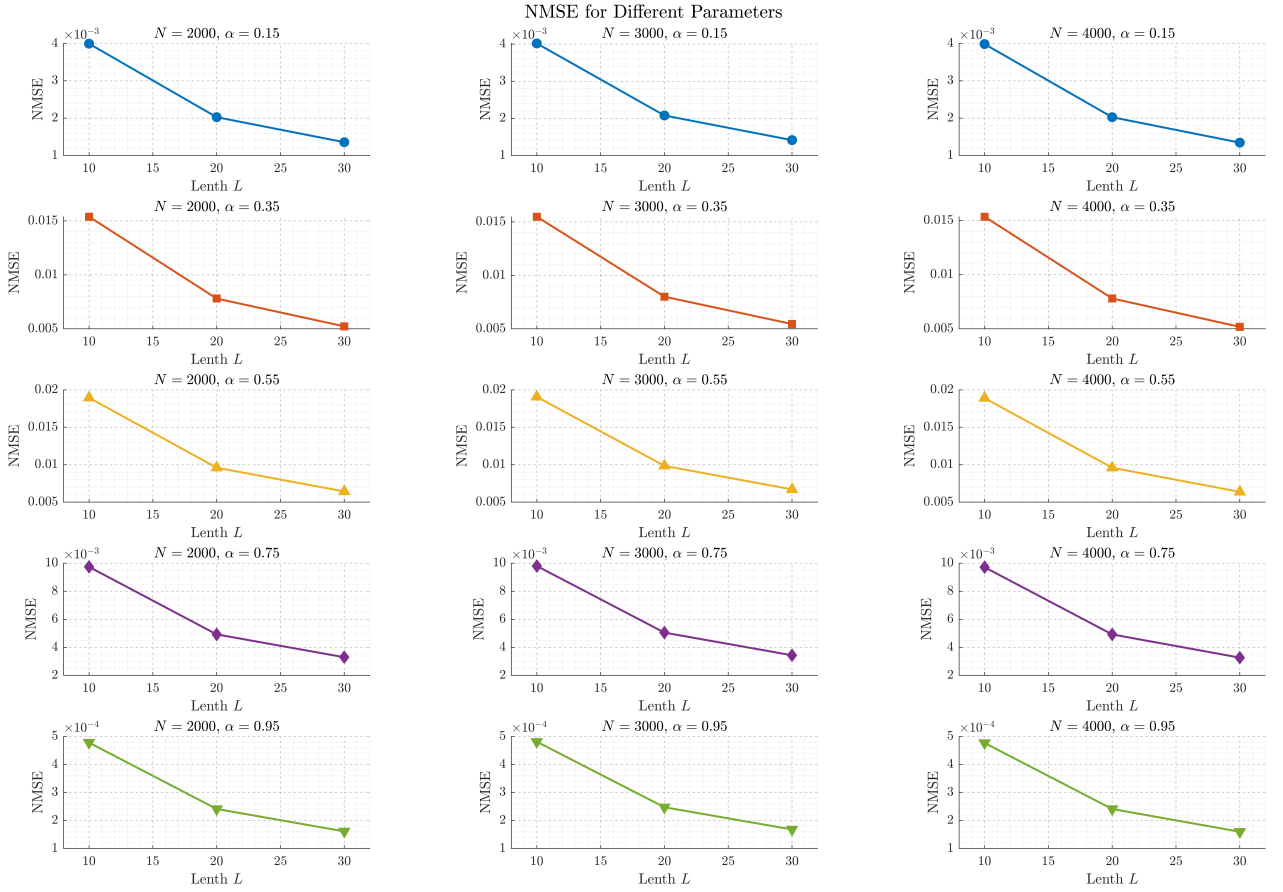


Fig. 4: The trend of NMSE with respect to truncation order L .

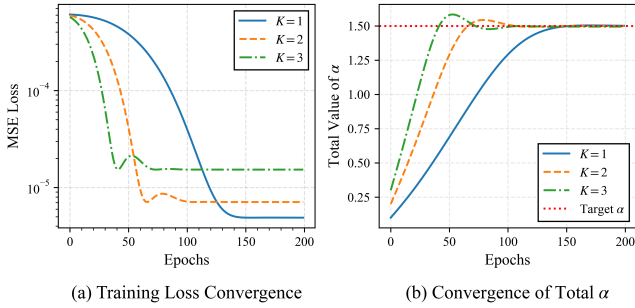


Fig. 5: Visualizations of the training process showing Loss curves and transform order update trajectories under different network layer counts.

B. Image and Point Cloud Denoising Based on Gradient Learning

To further verify the practical utility and computational advantages of the proposed FGFRFT algorithm in large-scale graph signal processing tasks, we model images and 3D point clouds as graph signals and apply them to denoising tasks. This experiment follows the existing gradient descent-based denoising model [25], aiming to jointly optimize the transform order α and the diagonal filter coefficients \mathbf{H} via the backpropagation algorithm, minimizing the error between the recovered signal and the ground truth, as shown in Eq. (23):

$$(\alpha^*, \mathbf{H}^*) = \operatorname{argmin}_{\alpha, \mathbf{H}} \|\mathbf{F}_G^{-\alpha} \mathbf{H} \mathbf{F}_G^\alpha \mathbf{y} - \mathbf{x}\|_2^2. \quad (27)$$

Unlike previous studies that focus on exploring the op-

timization strategy itself, the core objective of this section is to verify whether replacing the computationally expensive exact GFRFT matrix with the proposed approximate FGFRFT matrix under the same optimization framework, as shown in Eq. (24), can significantly reduce processing time while maintaining denoising performance:

$$(\alpha^*, \mathbf{H}^*) = \operatorname{argmin}_{\alpha, \mathbf{H}} \|\mathbf{Q}_L^{-\alpha} \mathbf{H} \mathbf{Q}_L^\alpha \mathbf{y} - \mathbf{x}\|_2^2. \quad (28)$$

In the image denoising experiment, we select standard images (256×256) from the Set12 dataset [39]. To accommodate memory constraints for graph signal processing, the images were split into non-overlapping 64×64 local patches. Each patch is flattened into a graph signal of dimension $N = 4096$, and a 4-nearest neighbor grid graph is constructed in the pixel space to form the adjacency matrix. Gaussian white noise with a standard deviation of $\sigma = 20.0$ was added to the experiments. The optimizer used is Adam with a learning rate of 0.01, and the training rounds were set to 300 epochs. The truncation order was set to $L = 10$, and the initial transform order α was set to 0.5. For comparison, the exact GFRFT method was run under identical graph structures and parameter settings. We present the visual results in Fig. 6 and the quantitative results in Table IV.

In the 3D point cloud denoising experiment, we select the microsoft voxelized dataset 3 [40] and adopt a preprocessing method similar to the image experiment. The point clouds are downsampled and split into multiple independent batches containing $N = 4000$ vertices. A denser 40-nearest neighbor graph structure is constructed based on Euclidean distance. The experiment was also conducted under a noise



Fig. 6: Visual comparison of image denoising performance on sample images from the Set12 dataset.

TABLE IV: Image Denoising Performance Comparison on Set12

Image	Standard GFRFT		Proposed FGFRFT		Improvement (PSNR)
	PSNR	SSIM	PSNR	SSIM	
Fig 1	39.222	0.9503	40.132	0.9691	+0.91 dB
Fig 2	38.499	0.9525	38.131	0.9598	-0.37 dB
Fig 3	39.925	0.9694	41.517	0.9900	+1.59 dB
Time Metric	Value		Value		Speedup
Avg Time / Batch	540 s		220 s		2.47×
Total Time	2.40 h		0.97 h		

TABLE V: 3D Point Cloud Denoising Performance Comparison (Microsoft Voxelized Dataset)

Point Cloud	Standard GFRFT		Proposed FGFRFT		Improvement (PSNR)
	PSNR (dB)		PSNR (dB)		
David9	37.10		40.85		+3.75 dB
Andrew9	38.95		39.26		+0.31 dB
Sarah9	42.63		42.96		+0.33 dB
Time Metric	Value		Value		Speedup
Avg Time / Batch	3900 s		1200 s		3.25×
Total Time	5.42 h		1.67 h		

level of $\sigma = 20.0$, with training rounds increase to 1000 epochs to ensure convergence; other hyperparameters remain consistent with the image experiment. We present the visual results in Fig. 7 and the quantitative results in Table V.

The experimental results demonstrate that the proposed FGFRFT algorithm achieves an excellent balance between denoising precision and computational efficiency. In the

image denoising task, the approximate algorithm not only avoid performance degradation due to series truncation but also achieve peak signal-to-noise ratios (PSNR) slightly higher than the exact GFRFT on some test samples. For instance, in Image 1, the PSNR of the FGFRFT reconstructed image reach 40.132 dB, slightly outperforming the standard method’s 39.222 dB. However, in terms of computational efficiency, FGFRFT exhibit significant advantages. By avoiding the $O(N^3)$ dense matrix operations in each iteration, the total training time for the image denoising task is drastically reduced from 2.4 hours for the standard method to 0.97 hours, and the average time per batch drop from 540 seconds to 220 seconds.

Similarly, in the 3D point cloud denoising task involving complex geometric structures, the proposed method demonstrate even more compelling superiority. On the David9 dataset, the PSNR of FGFRFT reach 40.85 dB, significantly surpassing the standard method’s 37.10 dB. Meanwhile, the total training time is compressed from 5.42 hours to 1.67 hours, achieving a speedup of approximately 3.25 times. These results strongly validate that the proposed approximation strategy can effectively reduce computational overhead while preserving, or even enhancing, signal reconstruction quality in complex manifolds. We provide the denoising source code in Algorithm 3 below.

C. Fractional Specformer Node Classification

To verify the effectiveness and compatibility of the proposed FGFRFT within deep learning frameworks, we

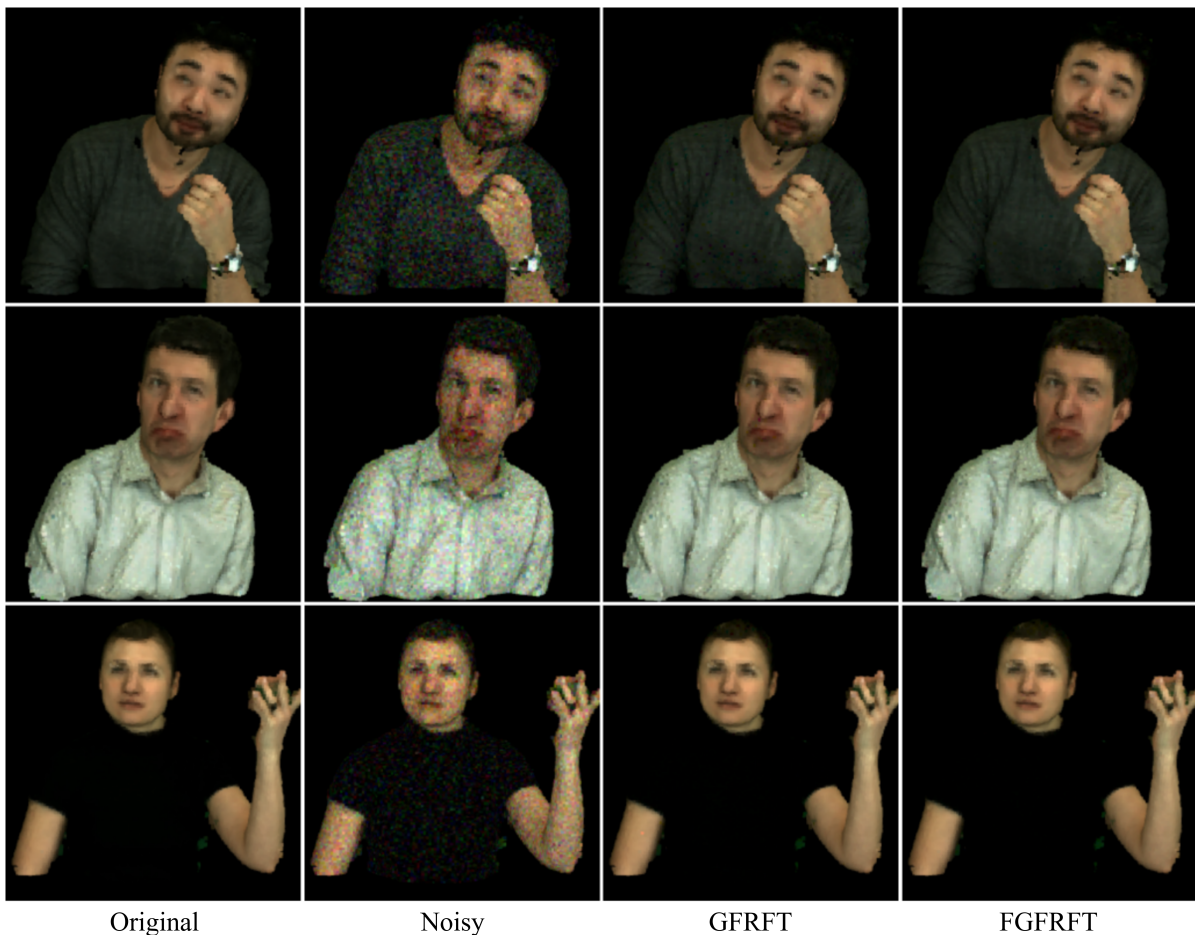


Fig. 7: Visual comparison of 3D point cloud denoising

integrate it into the existing state-of-the-art graph neural network architecture. Specformer utilizes the self-attention mechanism of transformers to adaptively learn spectral filters [30]. However, its original architecture is based on the standard GFT and is limited by a fixed orthogonal basis. This section proposes the fractional specformer, which replaces the GFT module with a learnable GFRFT module, enhancing the model’s ability to extract features from complex graph signals and verifying the efficiency advantages of the fast algorithm in large-scale model learning tasks.

Specformer transforms graph data from the spatial domain to the graph spectral domain by introducing spectral filters, thereby capturing both global structure and local features of the graph data.

$$\mathbf{H}_{out} = \sum_{h=1}^H \mathbf{F}_G \cdot \text{diag}(\mathbf{w}_h) \cdot \mathbf{F}_G^{-1} \cdot \mathbf{H}_{in}, \quad (29)$$

where \mathbf{w}_h represents the filter coefficients learned by the h -th attention head, and $\mathbf{H}_{in} \in \mathbb{R}^{N \times d_{in}}$ and $\mathbf{H}_{out} \in \mathbb{R}^{N \times d_{out}}$ denote the input and output node feature matrices, respectively, with N being the number of nodes. We replace the GFT matrix in Eq. (29) with the GFRFT matrix. The improved layer propagation formula is defined as:

$$\mathbf{H}_{out} = \sum_{h=1}^H \mathcal{T}^{-\alpha} \cdot \text{diag}(w_h) \cdot \mathcal{T}^{\alpha} \cdot \mathbf{H}_{in}, \quad (30)$$

where \mathcal{T}^{α} and $\mathcal{T}^{-\alpha}$ represent the GFRFT and inverse transform matrices, respectively. α is set as a learnable

parameter, allowing the model to automatically learn the optimal graph fractional domain representation during the training process. The experiment compares the following three variants:

- **GFT-Based:** Original architecture with $\alpha = 1$, i.e., $\mathcal{T}^{\alpha} = \mathbf{F}_G$.
- **GFRFT-Based:** Adopts the exact fractional transform matrix based on eigendecomposition, $\mathcal{T}^{\alpha} = \mathbf{F}_G^{\alpha}$.
- **FGFRFT-Based:** Adopts the proposed FGFRFT matrix, $\mathcal{T}^{\alpha} = \mathbf{Q}_L^{\alpha}$.

We conduct semi-supervised node classification tasks on six public benchmark datasets, including three homophilic graphs (Cora, Citeseer, Photo) and three heterophilic graphs (Chameleon, Squirrel, Actor). The evaluation metrics include classification accuracy and training time per epoch. Regarding hyperparameter selection, we performed fine-tuning based on the source code, with the initial value of α set to 1. The results are shown in Table VI.

Experimental data indicate that introducing the fractional transform mechanism significantly improves the model’s classification performance. Across all six datasets, the accuracy of the GFRFT-Based method consistently outperforms the GFT-Based baseline. This performance improvement is particularly evident on heterophilic graph datasets; for instance, on the Squirrel dataset, the accuracy improve from 63.51% to 64.19%. This result confirms that the fractional order parameter α provides additional degrees of freedom, enabling the model to adapt more flexibly to different types of graph topological structures.

TABLE VI: Performance Comparison on Node Classification: Accuracy (%) and Training Time (s/epoch)

Method	Metric	Homophilic			Heterophilic		
		Cora	Citeseer	Photo	Chameleon	Squirrel	Actor
GFT-Based	Acc	87.21±0.57	80.34±1.19	94.47±0.48	75.40±1.67	63.51±1.32	41.56±0.81
	Time	0.41	0.33	3.47	0.30	1.44	1.64
GFRFT-Based	Acc	87.45±0.62	80.67±1.42	94.47±0.47	76.13±1.47	64.19±1.12	41.79±1.10
	Time	1.46	2.75	22.18	1.09	8.78	9.84
FGFRFT-Based	Acc	87.49±0.62	80.48±1.35	94.50±0.43	76.15±1.30	64.50±1.29	41.84±1.09
	Time	0.76	0.67	5.90	0.84	4.21	2.79

Note: The best accuracy results are highlighted in bold. The proposed FGFRFT method achieves competitive accuracy with significantly reduced training time compare to the exact implementation.

Algorithm 2 Transform Order Learning Network

Require: Graph Shift Operator \mathbf{Z} , Input Signal \mathbf{X} , Target Order α_{target} , Network Depth K , Truncation L , Learning Rate η .

Ensure: Learned orders $\{\alpha_l\}_{l=1}^K$ and Total Order α_{sum} .

- 1: **Initialization:**
- 2: $\mathbf{Y} \leftarrow \mathbf{F}_G^{\alpha_{target}} \mathbf{X}$.
- 3: Initialize learnable parameters: $\alpha = [\alpha_1, \dots, \alpha_K]$ with $\alpha_l \leftarrow 0.1$.
- 4: **Pre-computation (Once):**
- 5: Execute **Stage 1** of Alg. 1 to obtain Basis Cache $\mathcal{C} = \{\mathbf{P}_n\}_{n=1}^L$.
- 6: **Training Loop:**
- 7: **for** $epoch = 1$ to E **do**
- 8: $\hat{\mathbf{X}}^{(0)} \leftarrow \mathbf{X}$
- 9: **for** $l = 1$ to K **do**
- 10: 1. *Operator Update (Stage 2 of Alg. 1)*
- 11: Compute layer operator $\mathbf{Q}_L^{\alpha_l}$ using Cache \mathcal{C} and current α_l .
- 12: 2. *Layer Transformation*
- 13: $\hat{\mathbf{X}}^{(l)} \leftarrow \mathbf{Q}_L^{\alpha_l} \cdot \hat{\mathbf{X}}^{(l-1)}$.
- 14: **end for**
- 15: Predicted Output: $\hat{\mathbf{Y}} \leftarrow \hat{\mathbf{X}}^{(K)}$.
- 16: Compute Loss: $\mathcal{L} \leftarrow \frac{1}{N^2} \|\hat{\mathbf{Y}} - \mathbf{Y}\|_2^2$.
- 17: Compute Gradients: $\nabla_{\alpha} \mathcal{L} \leftarrow \frac{\partial \mathcal{L}}{\partial \alpha}$ via Automatic Differentiation.
- 18: Update Parameters: $\alpha \leftarrow \text{Adam}(\alpha, \nabla_{\alpha} \mathcal{L}, \eta)$.
- 19: **end for**
- 20: **Result Aggregation:**
- 21: $\alpha_{sum} \leftarrow \sum_{l=1}^K \alpha_l$.
- 22: **return** α_{sum} .

Although the GFRFT-Based method brings accuracy gains, its computational cost is extremely high. As shown in Table VI, the training time of the GFRFT-Based method is typically multiples of the baseline method; for example, it increase by approximately 6 times on the Photo dataset. In contrast, FGFRFT-Based significantly reduces computational overhead while maintaining high accuracy. Benefiting from the low-complexity characteristics of the algorithm, the training time of FGFRFT-Based on the Squirrel dataset is only 48% of that of GFRFT-Based, and it achieves nearly a 4x speedup on the Photo dataset. Furthermore, experimental results show that the classification accuracy of the FGFRFT-

Algorithm 3 FGFRFT Denoising

Require: Noisy signal \mathbf{y} , Reference signal \mathbf{x} , Graph Shift Operator \mathbf{Z} , Truncation order L .

Require: Hyperparameters: Learning rate η , Max epochs T_{max} .

Ensure: Optimal fractional order α^* and Filter \mathbf{H}^* .

- 1: **Initialization:**
- 2: Initialize parameters: $\alpha^{(0)}$ (random or specific), $\mathbf{H}^{(0)}$ (e.g., Identity \mathbf{I}_N).
- 3: Set best metrics: $\mathcal{L}_{min} \leftarrow +\infty$, $\alpha^* \leftarrow \alpha^{(0)}$, $\mathbf{H}^* \leftarrow \mathbf{H}^{(0)}$.
- 4: **Pre-computation (Once):**
- 5: Execute **Stage 1** of Alg. 1 to obtain Basis Cache $\mathcal{C} = \{\mathbf{P}_n\}_{n=1}^L$.
- 6: **Optimization Loop:**
- 7: **for** $t = 0$ to $T_{max} - 1$ **do**
- 8: *Step 1: Operator Construction*
- 9: Construct forward operator $\mathbf{Q}_L^{\alpha^{(t)}}$ using Cache \mathcal{C} (via Alg. 1 Stage 2).
- 10: *Step 2: Fractional Domain Filtering*
- 11: Compute filtered signal:
- 12: $\tilde{\mathbf{x}}^{(t)} \leftarrow (\mathbf{Q}_L^{\alpha^{(t)}})^H \cdot \mathbf{H}^{(t)} \cdot \mathbf{Q}_L^{\alpha^{(t)}} \cdot \mathbf{y}$.
- 13: *Step 3: Loss Evaluation*
- 14: $\mathcal{L}^{(t)} \leftarrow \|\tilde{\mathbf{x}}^{(t)} - \mathbf{x}\|_2^2$.
- 15: **if** $\mathcal{L}^{(t)} < \mathcal{L}_{min}$ **then**
- 16: $\mathcal{L}_{min} \leftarrow \mathcal{L}^{(t)}$, $\alpha^* \leftarrow \alpha^{(t)}$, $\mathbf{H}^* \leftarrow \mathbf{H}^{(t)}$.
- 17: **end if**
- 18: *Step 4: Parameter Update (Gradient Descent)*
- 19: Compute gradients: $\nabla_{\mathbf{H}} \mathcal{L}^{(t)}$, $\nabla_{\alpha} \mathcal{L}^{(t)}$ via Auto-Diff.
- 20: $\mathbf{H}^{(t+1)} \leftarrow \mathbf{H}^{(t)} - \eta \nabla_{\mathbf{H}} \mathcal{L}^{(t)}$.
- 21: $\alpha^{(t+1)} \leftarrow \alpha^{(t)} - \eta \nabla_{\alpha} \mathcal{L}^{(t)}$.
- 22: **end for**
- 23: **return** α^*, \mathbf{H}^*

Based method is highly consistent with that of the GFRFT-Based method, and even slightly superior on some datasets, demonstrating the numerical robustness and practical value of this approximate algorithm in deep learning tasks.

VI. CONCLUSION

This study address the bottlenecks of the high computational complexity ($O(N^3)$) of GFRFT on large-scale graph data and its difficulty in being embedded into deep

learning frameworks, proposing a fast, differentiable approximation algorithm named FGFRFT. By leveraging Fourier series approximation combined with an efficient matrix power caching strategy, we successfully reduce the on-line computational complexity to $O(N^2)$, breaking through the computational barrier of traditional methods based on eigendecomposition. This provides an efficient, flexible, and theoretically rigorous bridge for integrating GSP and graph deep learning. Although FGFRFT significantly improves computational efficiency, it essentially adopts a space-for-time strategy, facing higher memory overhead and pre-computation costs when processing ultra-large-scale graphs. Future research will focus on optimizing sparse matrix storage and dynamic caching mechanisms to further alleviate storage pressure and enhance the algorithm's scalability.

REFERENCES

- [1] D. I. Shuman, S. K. Narang, P. Frossard, A. Ortega, and P. Vandergheynst, "The emerging field of signal processing on graphs: Extending high dimensional data analysis to networks and other irregular domains," *IEEE Signal Processing Magazine*, vol. 30, no. 3, pp. 83–98, 2013.
- [2] A. Sandryhaila and J. M. F. Moura, "Big data analysis with signal processing on graphs: Representation and processing of massive data sets with irregular structure," *IEEE Signal Processing Magazine*, vol. 31, no. 5, pp. 80–90, 2014.
- [3] M. Onuki, S. Ono, M. Yamagishi, and Y. Tanaka, "Graph signal denoising via trilateral filter on graph spectral domain," *IEEE Transactions on Signal and Information Processing over Networks*, vol. 2, no. 2, pp. 137–148, 2016.
- [4] L. Stankovic, D. Mandic, M. Dakovic, M. Brajovic, B. Scalzo, and T. Constantinides, "Graph signal processing – Part I: Graphs, graph spectra, and spectral clustering," *arXiv preprint arXiv:1907.03467*, 2019.
- [5] S. K. Narang and A. Ortega, "Compact support biorthogonal wavelet filterbanks for arbitrary undirected graphs," *IEEE Transactions on Signal Processing*, vol. 61, no. 19, pp. 4673–4685, 2013.
- [6] S. Chen, R. Varma, A. Sandryhaila, and J. Kovačević, "Discrete signal processing on graphs: sampling theory," *IEEE Transactions on Signal Processing*, vol. 63, no. 24, pp. 6510–6523, Dec. 2015.
- [7] S. K. Narang and A. Ortega, "Perfect reconstruction two-channel wavelet filter banks for graph structured data," *IEEE Transactions on Signal Processing*, vol. 60, no. 6, pp. 2786–2799, 2012.
- [8] A. Anis and A. Ortega, "Towards a sampling theorem for signals on arbitrary graphs," in *Proceedings of IEEE International Conference on Acoustics, Speech and Signal Processing (ICASSP)*, May 2014, pp. 3864–3868.
- [9] P. Hu and W. C. Lau, "A survey and taxonomy of graph sampling," *Computer Science*, Aug. 2013.
- [10] S. Chen, A. Sandryhaila, J. M. F. Moura, and J. Kovačević, "Signal recovery on graphs: Variation minimization," *IEEE Transactions on Signal Processing*, vol. 63, no. 17, Sept. 2015.
- [11] S. K. Narang and A. Ortega, "Signal recovery on graphs: fundamental limits of sampling strategies," *IEEE Transactions on Signal and Information Processing over Networks*, vol. 2, no. 4, pp. 539–554, Dec. 2016.
- [12] F. Yan and B. Li, "Windowed fractional Fourier transform on graphs: Properties and fast algorithm," *Digital Signal Processing*, vol. 118, p. 103210, Nov. 2021.
- [13] F. Yan, W. Gao, and B. Li, "Windowed fractional Fourier transform on graphs: Fractional translation operator and Hausdorff-Young inequality," in *Proceedings of APSIPA Annual Summit and Conference (APSIPA ASC)*, 2020, pp. 255–259.
- [14] F. Yan and B. Li, "Spectral graph fractional Fourier transform for directed graphs and its application," *Signal Processing*, vol. 210, p. 109099, Sep. 2023.
- [15] Y. Zhang and B. Li, "The graph fractional Fourier transform in Hilbert space," *IEEE Transactions on Signal and Information Processing over Networks*, vol. 11, pp. 242–257, 2025.
- [16] D. Wei and Z. Yan, "Generalized sampling of graph signals with the prior information based on graph fractional Fourier transform," *Signal Processing*, vol. 214, p. 109263, Jan. 2024.
- [17] D. Wei and S. Yuan, "Hermitian random walk graph Fourier transform for directed graphs and its applications," *Digital Signal Processing*, vol. 155, p. 104751, Dec. 2024.
- [18] T. Alikashioglu, B. Kartal, and A. Koç, "Wiener filtering in joint time-vertex fractional Fourier domains," *IEEE Signal Processing Letters*, vol. 31, pp. 1319–1323, 2024.
- [19] Y. Wang, B. Li, and Q. Cheng, "The fractional Fourier transform on graphs," in *Proceedings of APSIPA Annual Summit and Conference (APSIPA ASC)*, 2017, pp. 105–110.
- [20] Y. Wang and B. Li, "The fractional fourier transform on graphs: Sampling and recovery," in *2018 14th IEEE International Conference on Signal Processing (ICSP)*, 2018, pp. 1103–1108.
- [21] C. Ozturk, H. M. Ozaktas, S. Gezici, and A. Koç, "Optimal fractional Fourier filtering for graph signals," *IEEE Transactions on Signal Processing*, vol. 69, pp. 2902–2912, 2021.
- [22] M. Cui, Z. Zhang, and W. Yao, "Graph chirp signal and graph fractional vertex–frequency energy distribution," *IEEE Transactions on Signal Processing*, vol. 73, pp. 5286–5302, 2025.
- [23] F.-J. Yan and B.-Z. Li, "Multi-dimensional graph fractional fourier transform and its application to data compression," *Digital Signal Processing*, vol. 129, p. 103683, 2022.
- [24] M. Cui, Z. Zhang, and W. Yao, "Multiple-parameter graph fractional fourier transform: Theory and applications," 2025. [Online]. Available: <https://arxiv.org/abs/2507.23570>
- [25] T. Alikashioglu, B. Kartal, and A. Koç, "Graph fractional Fourier transform: A unified theory," *IEEE Transactions on Signal Processing*, vol. 72, pp. 3834–3850, 2024.
- [26] Z. Yan and Z. Zhang, "Trainable joint time-vertex fractional Fourier transform," *Digital Signal Processing*, vol. 173, p. 105909, 2026.
- [27] F. Zhao, Y. He, and Z. Zhang, "Angular graph fractional Fourier transform: Theory and application," *arXiv preprint arXiv:2511.16111*, 2025.
- [28] C. Sheng, Z. Zhang, and W. Yao, "Graph embedding in the graph fractional fourier transform domain," 2025. [Online]. Available: <https://arxiv.org/abs/2508.02383>
- [29] D. Li and Z. Zhang, "Graph fractional Hilbert transform: Theory and application," *Fractal and Fractional*, vol. 10, no. 2, 2026.
- [30] D. Bo, C. Shi, L. Wang, and R. Liao, "Specformer: Spectral graph neural networks meet transformers," in *Proceedings of International Conference on Learning Representations (ICLR)*, 2023.
- [31] A. Sandryhaila and J. M. F. Moura, "Discrete signal processing on graphs," *IEEE Transactions on Signal Processing*, vol. 61, no. 7, pp. 1644–1656, 2013.
- [32] A. H. Ghodrati and M. A. Hosseinzadeh, "Signless Laplacian spectrum of a graph," *Linear Algebra and its Applications*, vol. 682, pp. 257–267, 2024.
- [33] F. Ji, W. P. Tay, and A. Ortega, "Graph signal processing over a probability space of shift operators," *IEEE Transactions on Signal Processing*, vol. 71, pp. 1159–1174, 2023.
- [34] F. Zhao and Z. Zhang, "Fractional graph spectral filtering based on unified graph representation matrix," *IEEE Signal Processing Letters*, 2025.
- [35] J. R. Partington, *Fourier Transforms and Complex Analysis*. Berlin, Heidelberg: Springer Berlin Heidelberg, 2006.
- [36] A. V. Oppenheim, A. S. Willsky, and S. H. Nawab, *Signals & systems*. Pearson Educación, 1997.
- [37] E. M. Stein and R. Shakarchi, *Fourier analysis: an introduction*. Princeton University Press, 2011, vol. 1.
- [38] K. W. Cattermole, *The Fourier transform and its applications*. IET, 1965.
- [39] "USC-SIPI image database," <https://sipi.usc.edu/database/>, accessed: 2026.
- [40] L. Charles, Q. Cai, E. S. Orts, and A. C. Philip, "JPEG pleno database: microsoft voxelized upper bodies-a voxelized point cloud dataset," 2021.